

SANDIA REPORT

SAND2013-8099

Unlimited Release

Printed September 2013

LDRD Project 151362: Low Energy Electron-Photon Transport

Ronald P. Kensek, Harold P. Hjalmarson, Rudolph J. Magyar,
Robert J. Bondi, and Martin J. Crawford

Prepared by
Sandia National Laboratories
Albuquerque, New Mexico 87185 and Livermore, California 94550

Sandia National Laboratories is a multi-program laboratory managed and operated by Sandia Corporation, a wholly owned subsidiary of Lockheed Martin Corporation, for the U.S. Department of Energy's National Nuclear Security Administration under contract DE-AC04-94AL85000.

Approved for public release; further dissemination unlimited.



Issued by Sandia National Laboratories, operated for the United States Department of Energy by Sandia Corporation.

NOTICE: This report was prepared as an account of work sponsored by an agency of the United States Government. Neither the United States Government, nor any agency thereof, nor any of their employees, nor any of their contractors, subcontractors, or their employees, make any warranty, express or implied, or assume any legal liability or responsibility for the accuracy, completeness, or usefulness of any information, apparatus, product, or process disclosed, or represent that its use would not infringe privately owned rights. Reference herein to any specific commercial product, process, or service by trade name, trademark, manufacturer, or otherwise, does not necessarily constitute or imply its endorsement, recommendation, or favoring by the United States Government, any agency thereof, or any of their contractors or subcontractors. The views and opinions expressed herein do not necessarily state or reflect those of the United States Government, any agency thereof, or any of their contractors.

Printed in the United States of America. This report has been reproduced directly from the best available copy.

Available to DOE and DOE contractors from

U.S. Department of Energy
Office of Scientific and Technical Information
P.O. Box 62
Oak Ridge, TN 37831

Telephone: (865) 576-8401
Facsimile: (865) 576-5728
E-Mail: reports@adonis.osti.gov
Online ordering: <http://www.osti.gov/bridge>

Available to the public from

U.S. Department of Commerce
National Technical Information Service
5285 Port Royal Rd.
Springfield, VA 22161

Telephone: (800) 553-6847
Facsimile: (703) 605-6900
E-Mail: orders@ntis.fedworld.gov
Online order: <http://www.ntis.gov/help/ordermethods.asp?loc=7-4-0#online>



SAND2013-8099
Unlimited Release
Printed September 2013

LDRD Project 151362: Low Energy Electron-Photon Transport

Ronald P. Kensek¹, Harold P. Hjalmarson¹, Rudolph J. Magyar²,
Robert J. Bondi³, and Martin J. Crawford¹

¹Radiation-Effects Theory Department

²Computational Shock and Multiphysics Department

³Radiation-Effects Research

Sandia National Laboratories

P.O. Box 5800

Albuquerque, New Mexico 87185-1179

Abstract

At sufficiently high energies, the wavelengths of electrons and photons are short enough to only interact with one atom at time, leading to the popular “independent-atom approximation”. We attempted to incorporate atomic structure in the generation of cross sections (which embody the modeled physics) to improve transport at lower energies. We document our successes and failures. This was a three-year LDRD project. The core team consisted of a radiation-transport expert, a solid-state physicist, and two DFT experts.

ACKNOWLEDGMENTS

This work was funded under LDRD Project Number 151362 and Title "Low Energy Electron-Photon Transport".

CONTENTS

1. Introduction.....	7
2. Photon Coherent Scattering	8
3. Electron elastic scattering	13
4. Photo-ionization cross sections.....	16
5. Electron inelastic scattering	17
7. Conclusions.....	21
8. Presentations:	22
9. References.....	24
Distribution	27

FIGURES

Figure 1. Existing atomic form factors from data within our transport code. The abscissa is related to momentum transfer (in units of inverse Angstroms), theta is angle of scatter and E is photon energy.....	8
Figure 2. Left: supercell (or repeat cell) of amorphous SiO ₂ containing 144 atoms. Center: radial distribution function, which is essentially the average number of nuclei per radial distance from any atom in the model. Right: radial density function, similar to the center plot, normalized per volume and per average atomic density (hence goes to unity at large radii).....	9
Figure 3. The square of the form factor for amorphous SiO ₂ , which is related to the photon coherent cross section as indicated on the ordinate. The measurement was from [Poulsen et al. 1995]. The green dashed curve is from the method described here. The smooth blue curve is the independent-atom approach.	10
Figure 4. Atomic models for polyethylene. Left: a single chain of an amorphous model. Center: all chains of the amorphous model. Right: a poly-crystalline model.	11
Figure 5. Anomalous spike in radial density function.	11
Figure 6. Form factor squared for polyethylene computed and compared with experiment.	12
Figure 7. Electron elastic scattering cross sections for U to verify use of ELSEPA code.....	13
Figure 8. Atomistic model of amorphous Ge.....	13
Figure 9. Electron elastic scattering cross sections. Red curves for amorphous Ge. Green curves for crystalline Ge. Smooth blue curve is independent-atom model.....	14
Figure 10. Electron elastic scattering cross sections in N ₂ for various energies generated with ELSEPA and compared with measurements [Jansen et al. 1976]. Calculations are with (solid curves) and without (dashed curves) the molecular logic in ELSEPA.....	15
Figure 11. The generalized oscillator strength surface for hydrogen.	17
Figure 12. The energy loss function for SiO ₂ . The red curve is our DFT calculation while the blue dots are measurements from [Palik 1985].....	18
Figure 13. Energy loss spectrum for SiO ₂ . Green curves are our attempt to use FEFF9 for the various labeled transitions. Blue dots are adapted from [Palik 1985].	18

Figure 14. The electron energy loss spectra near the edge transition for Si L. The green curves are our calculations using FEFF9 for Si L3 (upper) and Si L2 (lower). The blue dots are adapted from measurements [Palik 1985] of the total transition..... 19

Figure 15. The electron energy loss spectra for SiO2. Red curve is our DFT calculation. Green curves are our FEFF9 calculations for individual transitions. Blue dots are adapted from measurements [Palik 1985]..... 20

TABLES

Table 1. Specified uncertainties for photo-ionization cross sections of the Evaluated Photon Data Library (Cullen et al. 1997). 7

1. INTRODUCTION

General-purpose electron/photon radiation transport codes have been successfully used to simulate radiation interactions in the keV-MeV energy range [for example Jenkins et al. (1988), Chapters 8, 9, 11 and 13]. With the development of powerful, low-energy radiation sources such

Table 1. Specified uncertainties for photo-ionization cross sections of the Evaluated Photon Data Library (Cullen et al. 1997).

Uncertainties of weighted independent-atom tables

Energy Range	Solid	Gas
0.01-0.1 keV	1000%	20%
0.1-0.5 keV	100-200%	10-20%
0.5-1 keV	10-20%	5%
1-5 keV	5%	5%

as the Z facility at Sandia National Laboratories [Spielman et al. 1998], there has been an increased interest in simulations at lower energies. Cross-section data libraries have also been generated [Cullen et al. 1997; Perkins et al. 1991] but with acknowledged large error bars as can be seen in Table 1.

There is nothing magical about 1 keV. Indeed, some of the existing cross sections are already known to be suspect. Codes such as EGS5 [Hirayama et al. 2005] have begun to incorporate selected measured cross sections to help address the problem. While that may work well for applications such as medical physics with a somewhat restricted material database, a more direct question is to what extent can such cross sections be calculated to be used in general-purpose codes, to produce more reliable results? One of the assumptions that breaks down is the independent atom approximation. Can we incorporate solid-state and/or molecular effects into our cross-section

calculations, given the detail that is now being demonstrated with some atomistic simulations [Bondi et al. 2010]?

We had intended to look at four cross sections: photon coherent scattering, electron elastic scattering, photo-ionization and electron inelastic scattering. Due to the challenging nature of the work, examining photo-ionization was dropped to focus more on the other three. Even then we fell short of our ambitious goals.

2. PHOTON COHERENT SCATTERING

Our radiation-transport code is ITS, the Integrated Tiger Series [Franke et al. 2009]. The existing model of photon coherent scattering is the product of the Thomson scattering cross section with an atomic form factor [Seltzer, 1991]. For a mixture or compound, a mix of atomic form factors is used. This procedure thereby ignores diffraction effects which alters the scattering. Diffraction effects can also arise from condensed matter when the wavelength of the photon becomes large enough for the photon to interact with more than one atom at a time.

The atomic form factor is essentially a Fourier transform of the electron density of an isolated atom. One obvious potential improvement would be to use the Fourier transform of the electron density of the material, thereby picking up molecular and/or solid-state effects. This seemed easy for a Density-Functional-Theory (DFT) approach, though our attempt failed. Speculation was the use of inconsistent assumptions (infinite medium due to repeat cell, “small” sample size, average over all orientations). This should be better understood.

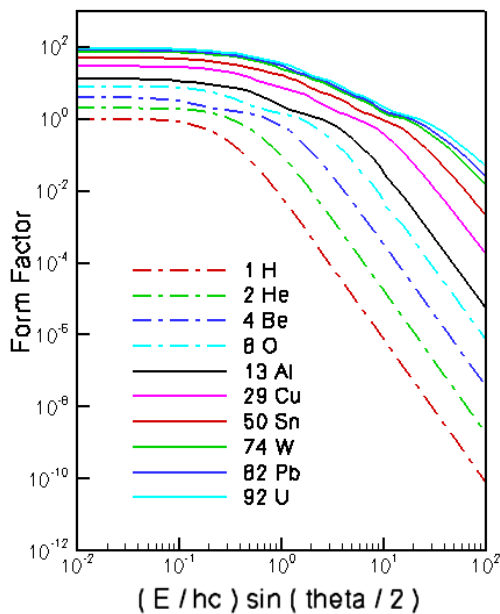


Figure 1. Existing atomic form factors from data within our transport code. The abscissa is related to momentum transfer (in units of inverse Angstroms), theta is angle of scatter and E is photon energy.

resources develop. People who have created such models may be eager to share their work or just as likely to guard something in which they invested so much of their time. One of our team members, Robert Bondi, had an amorphous SiO₂ model from previous work [Bondi et al. 2010], created an amorphous germanium model for this project, and acquired several other models including ones for polyethylene (both amorphous [Tsige et al. 2003] and semi-crystalline

While we were trying to come to a consensus of terminology, conventions, units, and goals, another approach was also attempted. X-ray diffraction has been used for a long time to infer atomic structure about a material. The idea would be to turn this around: to use the atomic structure of the material to generate the x-ray diffraction (i.e. the photon coherent scattering cross section). The simplification (which avoids the need for something like DFT) is to essentially use atomic electron densities superposed on the distribution of nuclei. The resulting Fourier transform will then a function of the atomic form factors, which are already utilized in our transport code (see Figure 1 for sample plots). Such calculations have been attempted, with the challenge being obtaining a good model of the atomic structure. Nowadays this could be obtained from an atomistic model of the material.

Good quality atomistic models are not quite routine (especially for complicated structures), but becoming more so as tools and computing

[Mattson et al. 2010]). I contacted Professor Zbigniew Stachurski who had created a model for Lucite about its availability. He encouraged me to use a commercial package called Materials Studio and otherwise follow the details in his paper. Although I did not follow up on his suggestion (the package is now \$2k a year – not appropriate for this project but something to keep in mind), I believe this indicates the trend of more available tools.

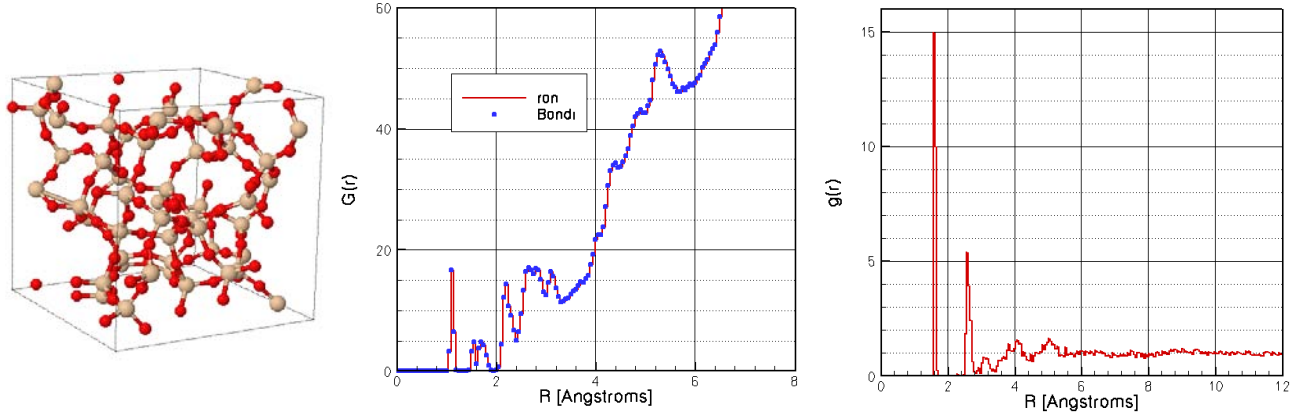


Figure 2. Left: supercell (or repeat cell) of amorphous SiO₂ containing 144 atoms. Center: radial distribution function, which is essentially the average number of nuclei per radial distance from any atom in the model. Right: radial density function, similar to the center plot, normalized per volume and per average atomic density (hence goes to unity at large radii).

Figure 2, left, shows an atomistic model (repeat cell) of amorphous SiO₂ containing 144 atoms. The model is large enough to capture amorphous aspects while being small enough to permit numerical DFT calculations [Bondi et al. 2010]. Figure 2, center, shows the radial distribution function which is commonly used in the literature. This is essentially the average number of nuclei per radial distance from any atom in the model and was useful for verifying our processing of the atomic model. Figure 2, right, is the radial density function, which we have found more useful. It is the same data as the center plot but now normalized per volume and per average atomic density so we can expect the oscillations to dampen out at large radii. The radial density function can be broken up into “partial” radial density functions $g_{IJ}(r)$ which give, for an atom of type I, the distribution (per volume) of atoms of type J.

The formalism of using x-ray diffraction measurements to infer atomic structure of materials has been discussed in [James 1947] and more recently in [Poulsen et al. 1995], which makes use of a “sharpening factor” discussed in [Warren 1990]. We reverse the process to obtain the molecular/solid-state form factor from the radial distribution functions from a Debye-like equation::

$$F_{mol}^2(x) = \sum_{I=1}^{NEL} \frac{N_I}{N_{ATOM}} N_{ApM} F_I^2(x) + \sum_{I=1}^{NEL} \sum_{J=1}^{NEL} \frac{N_I N_J}{N_{ATOM}} N_{ApM} F_I(x) F_J(x) \int_0^{\infty} 4\pi\rho [g_{IJ}(r) - 1] \frac{\sin(4\pi xr)}{4\pi xr} r^2 dr$$

NEL is the number of elements (distinct atoms) in the model repeat cell, N_{ATOM} is the total number of atoms in the cell, N_I is the number of atoms of type I in the cell, N_{APM} is the number of atoms per molecule (a normalization constant), $F_I(x)$ is the atomic form factor of atom type I, $x = \left(\frac{E}{hc}\right) \sin\left(\frac{\theta}{2}\right)$ is related to the momentum transfer, E is the energy of the photon, θ is the scattering angle, and $g_{IJ}(r)$ is the partial radial density function for atom of type I having neighbors of type J. Again, $g_{IJ}(r)$ is input from the processed atomistic model.

The above integral is handled as follows. From the processing of the model repeat cell, the partial radial density functions are tallied as histograms – constant in radius within a radial bin. We have finite data for the partials and while $g_{IJ}(r)$ approaches unity for large radii, the oscillations never completely stop. So a “convergence factor” of $\exp[-(a/r/r_{\text{MAX}})^2]$ is introduced as discussed in [Warren 1990] with $a=1.5$. Within a radial bin, this is approximated by the value at the midpoint, so the remaining parts of the integral may be done analytically. The integral is then replaced by a sum over radial bins. The molecular/solid-state form factor is evaluated on a grid of x (related to momentum transfer) points. At large x , the assumption is that oscillations die out and the usual independent-atom form factor formalism may be used.

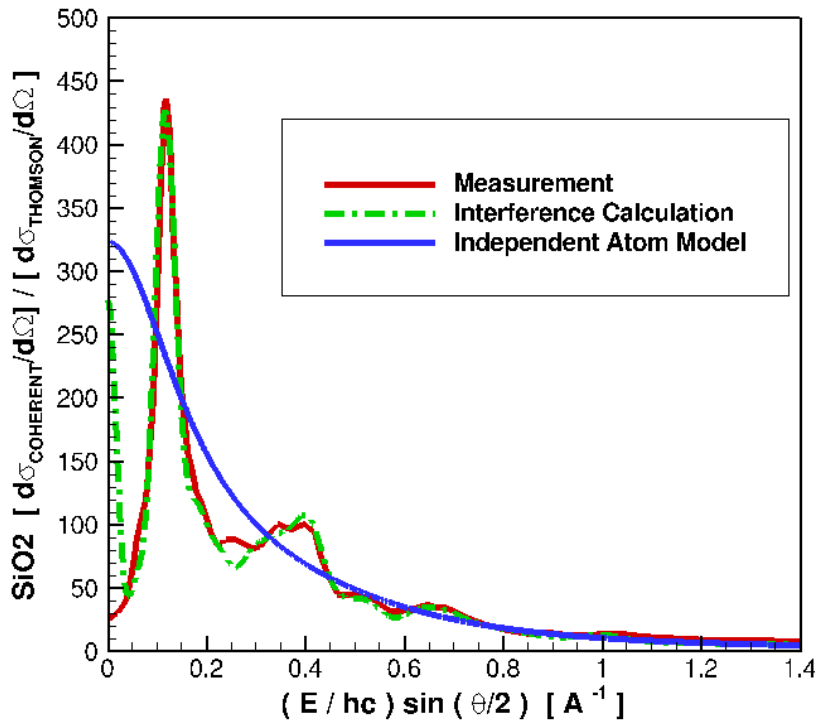


Figure 3. The square of the form factor for amorphous SiO₂, which is related to the photon coherent cross section as indicated on the ordinate. The measurement was from [Poulsen et al. 1995]. The green dashed curve is from the method described here. The smooth blue curve is the independent-atom approach.

Figure 3 show our results for amorphous SiO₂. Perhaps the excellent agreement is partly due to the use of 1.5 in the convergence factor (which was optimized for SiO₂), though it should be of order unity. The abscissa is related to the momentum transfer – for a given value of photon

energy E , it yields a distribution of scatter angles. Theoretically, there is a narrow spike at small momentum transfer – which is for small angles. The spike shown is likely an artifact of the numerical procedure utilizing (necessarily) finite radial information.

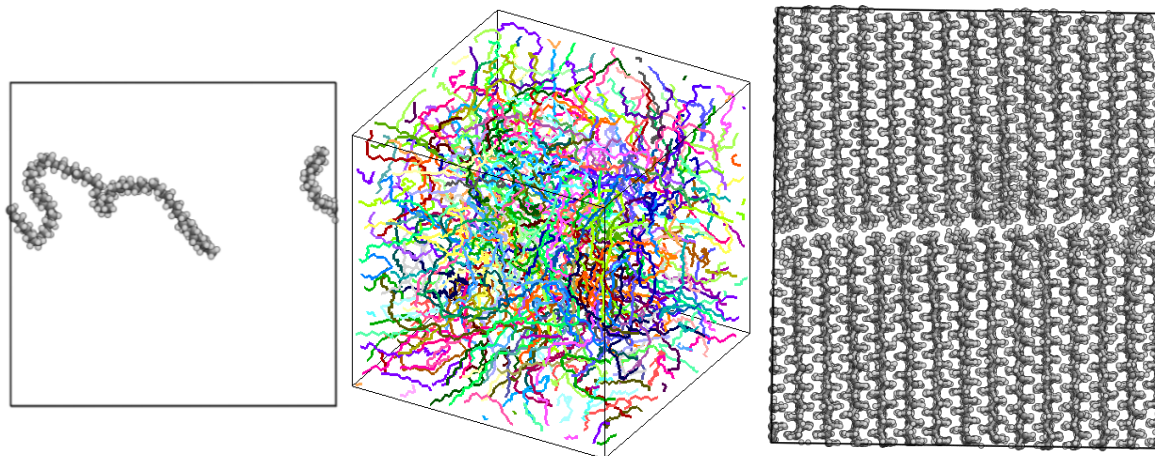


Figure 4. Atomic models for polyethylene. Left: a single chain of an amorphous model. Center: all chains of the amorphous model. Right: a poly-crystalline model.

To test this out on a more complicated case, we obtained atomic models for polyethylene, shown in Figure 4. It turns out common polyethylene is semi-crystalline, so that is the model we ended up using. There are 168 chains of $C_{44}H_{88}$ which is too large for a present-day DFT calculation, but can still be handled in the present formalism.

The form factor for polyethylene is quite narrow. It was recommended that one needs good radial distribution functions out to large radii to capture this. We attempted to go out to 100 Angstroms by repeating the unit cell as needed. Examining the distribution near 100 Angstroms, to see how flat it was, revealed an interesting spike as shown in Figure 5.

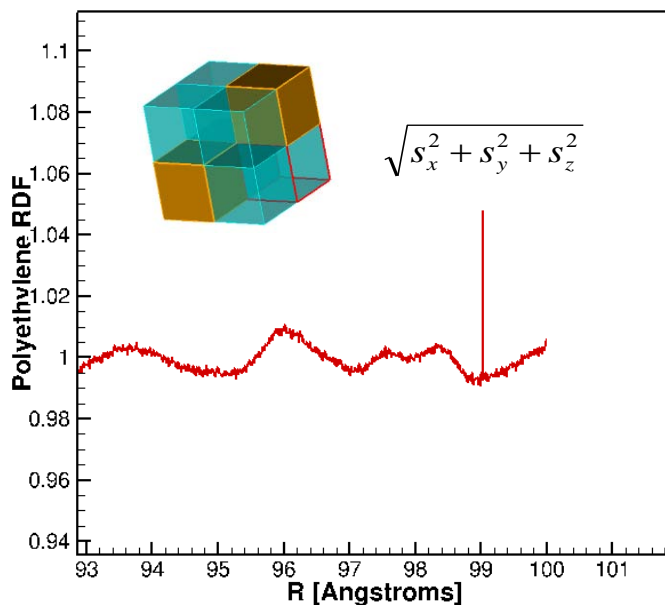


Figure 5. Anomalous spike in radial density function.

This is an artifact of repeating the unit cell within this procedure. When one atom sees a copy of itself, all of the atoms in that cell also see a copy of itself at the same distance. In fact, the spike near 100 Angstroms was due to a copy kitty-corner as shown as an insert in Figure 5. Once understood, it was easy to locate other such spikes corresponding to neighboring cells laterally and diagonally.

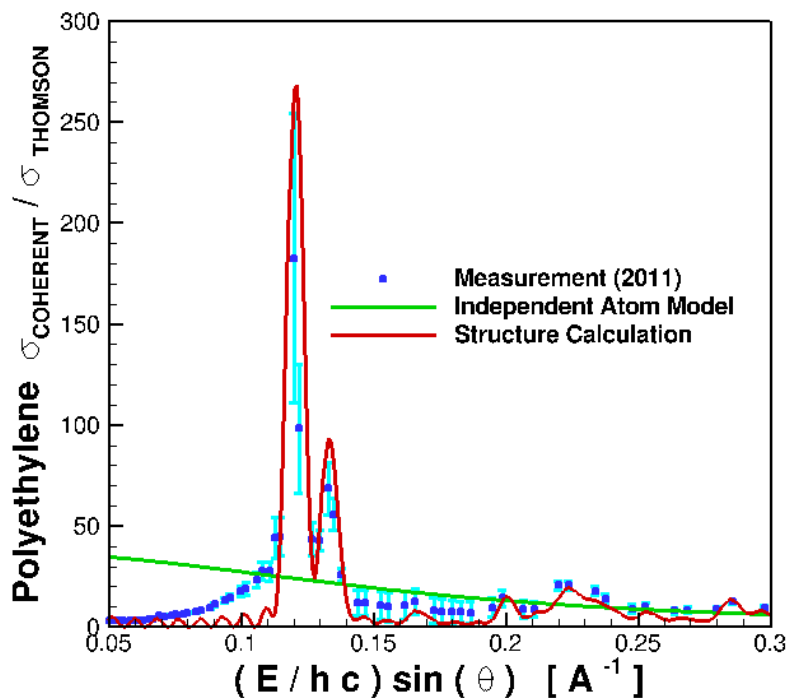


Figure 6. Form factor squared for polyethylene computed and compared with experiment.

Figure 6 shows our results for semi-crystalline polyethylene compared with experiment [King et al. 2011] and the independent-atom model. While the agreement is not as good, the trend is certainly more in agreement than the independent-atom model.

3. ELECTRON ELASTIC SCATTERING

Much work has been done on electron elastic scattering [ICRU 2007] and code is available which can even treat small molecules [Salvat et al. 2005]. We decided to use this as a starting point of our investigations. It turns out DFT calculations are not appropriate for electron cross sections.

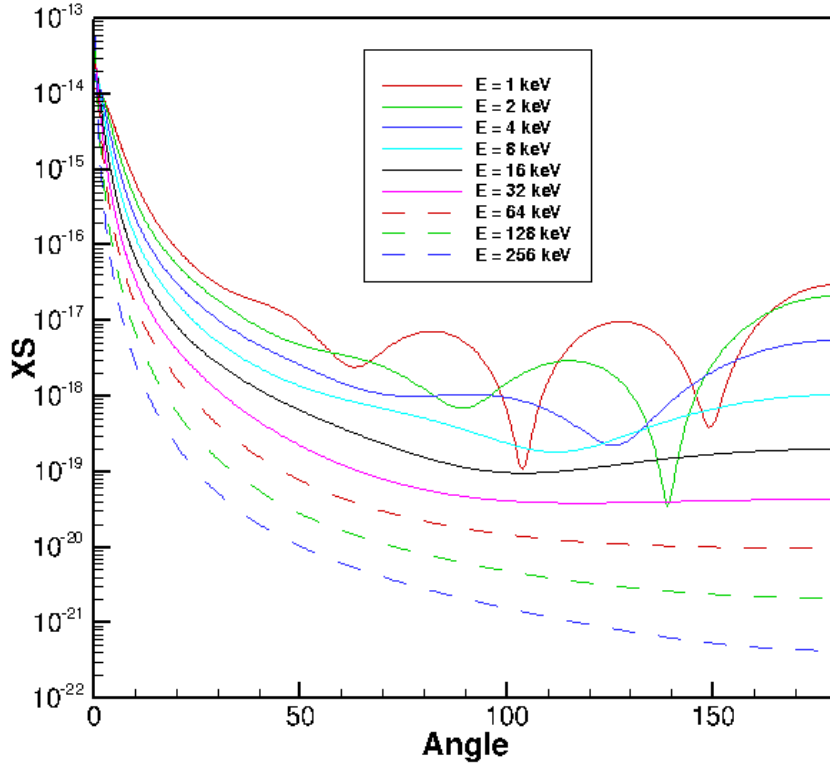


Figure 7. Electron elastic scattering cross sections for U to verify use of ELSEPA code.

We obtained the code and generated electron elastic scattering cross sections from 1-256 keV electrons on U. We compared those with existing cross sections used in our ITS transport code – in fact we tried to use comparable options in ELSEPA to mimic how the ITS cross sections were generated. Agreement was excellent with a maximum disagreement of a couple percent.

We were aware of some measurements [Brunger and Menz 1965] on Ge (both amorphous and crystalline) demonstrating diffraction effects. An amorphous atomistic model of Germanium was created for this project. The ELSEPA code was modified to take the coordinates of the atoms as input (essentially increasing appropriate array sizes). The code treated the supercell as one large molecule. The results in Figure 9 were promising (for such a simple change) as far as capturing oscillations corresponding to the oscillations shown in the measurements (and completely missing in the independent-atom model calculation).

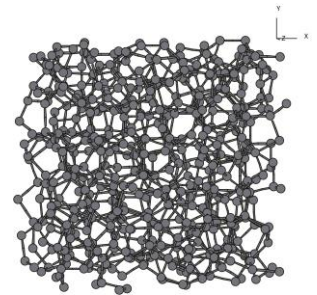


Figure 8. Atomistic model of amorphous Ge.

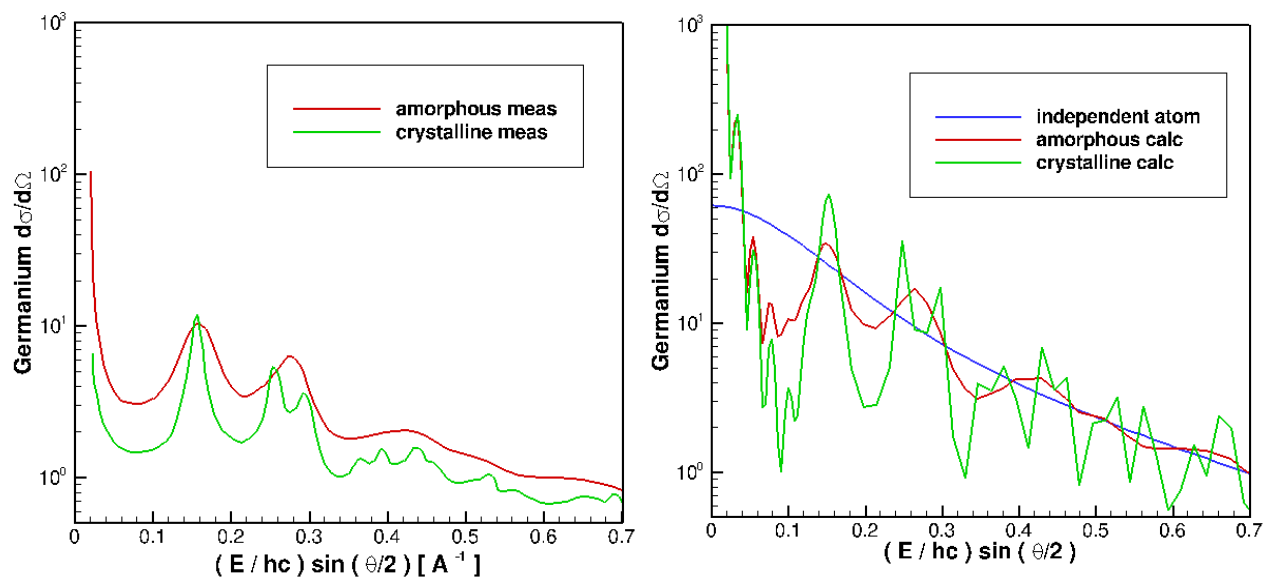


Figure 9. Electron elastic scattering cross sections. Red curves for amorphous Ge. Green curves for crystalline Ge. Smooth blue curve is independent-atom model. Left: Measurements [Brunger and Menz 1965]. Right present calculations.

The next step was to attempt to improve the magnitude of the cross sections. Notice the calculations are essentially following the independent-atom curve. The method of solution within the ELSEPA code involves solving the radial Dirac equations for phase-shifts which create the cross section. The potential used for the wave functions are still those of individual atoms. The idea was to use a radially averaged potential which is due to more than just a single atom, but that seen in our atomistic model. This produces a net potential which changes sign as neighboring nuclei are passed. We convolved a muffin-tin electron density for a single atom with the radial distribution function of the Ge nuclei. However, we were unsuccessful in demonstrating any positive effect in the resulting calculations.

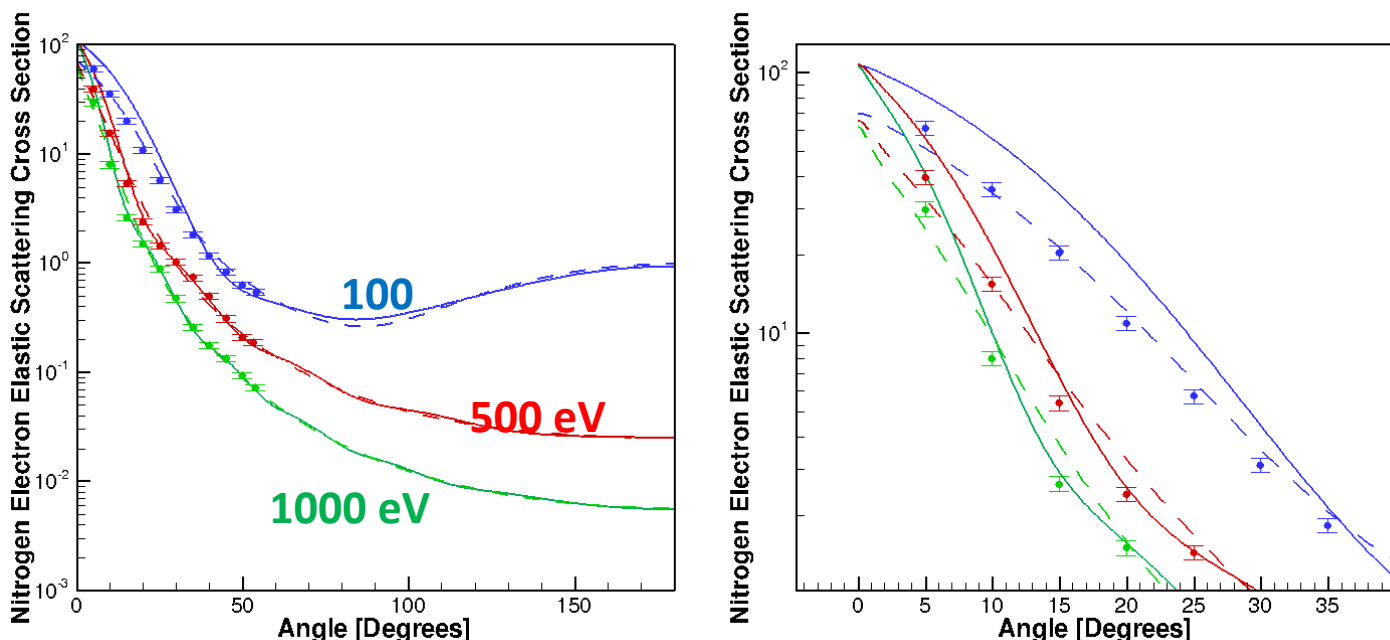


Figure 10. Electron elastic scattering cross sections in N₂ for various energies generated with ELSEPA and compared with measurements [Jansen et al. 1976]. Calculations are with (solid curves) and without (dashed curves) the molecular logic in ELSEPA.

We also looked at electron elastic scattering in nitrogen (an application of some interest to us) and compared with measurements as shown in Figure 10. Here, we could use ELSEPA with no modifications. The intent was to demonstrate better results by using the built-in algorithms to handle small molecules. However, the results were quite disappointing. While at large angles (Figure 10 Left) indicated little difference, the differences apparent in the small-angle plot (Figure 10 Right) suggest it may be better to avoid using the molecular logic at least for this data set.

4. PHOTO-IONIZATION CROSS SECTIONS

Due to underestimating the difficulties encountered for our challenging goals, we made a course correction and decided not to spend time investigating photon-ionization cross sections. We did obtain the FEFF9 code [Rehr et al. 2010] which can generate such cross sections and indeed can calculate such things as fine structure near edges. Other papers [Jorissen et al. 2010] [Sorini et al. 2006] have used it to generate results related to low-energy electron cross sections (which motivated our obtaining the tool). We did reproduce a copper example of fine structure.

However, apparently FEFF9 does not get the branching ratios correct for, say L shell transitions and there are cautions for generating say M-shell transitions. Also, we were having trouble generating the results we wanted (though this could simply be our inexperience with the code). So we still have much to learn to be able to confidently apply the tool.

5. ELECTRON INELASTIC SCATTERING

Electron inelastic scattering cross sections are doubly differential in energy loss and scattering angle. In principle this can be obtained from the generalized oscillator surface (GOS) which, in turn, is related to the imaginary part of the reciprocal of the dielectric function. For illustrative purposes, the GOS for hydrogen (the only atom for which an analytic result is possible) is shown in Figure 11.

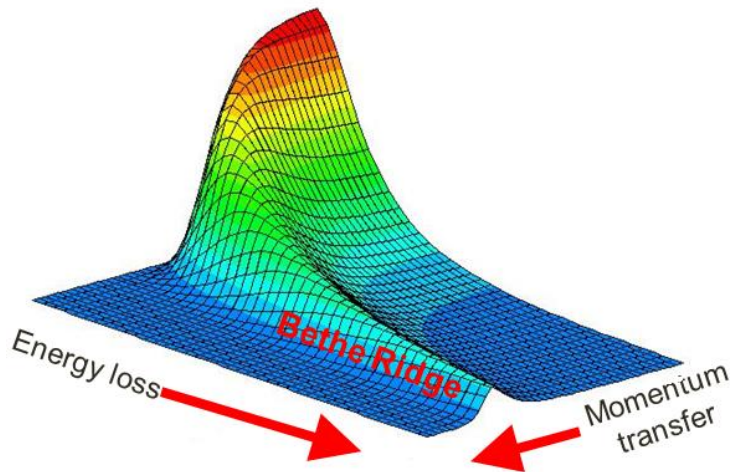


Figure 11. The generalized oscillator strength surface for hydrogen.

The curve at zero momentum transfer is related to the energy loss function. This is the reciprocal of the dielectric function at zero momentum transfer and can be expressed in terms of the real and imaginary parts of the index of refraction (hence “optical” data). A prominent feature of the GOS is the “Bethe Ridge” at both large energy loss and large momentum transfer. This is due to the close collisions (or “hard” or “catastrophic” collisions).

At first, we thought we could simply perform a DFT calculation to determine the complex dielectric function as a function of energy loss and momentum transfer, but as already pointed out [Plagemann et al. 2012] “...the *ab initio* approach is so far only applicable for wavenumbers $k=0$...” This leads to approaches whereby the energy loss function is obtained (traditionally by measurement) together with some approach to extrapolate into $k>0$. While the extrapolation procedure is necessarily imprecise, it is constrained to obey certain constraints (sum rules).

Instead of relying on experimental measurements, we intended to calculate the energy loss function. This is already being done with the FEF9 code (as previously mentioned in the section on Photoionization). We obtained this code to apply to our SiO₂ atomistic model. At the same time, we decided to use a DFT calculation to compare the results. (It was pointed out this may also be obtained at small energy loss through band-structure calculations.) Figure 12 shows our DFT calculations compared with measurements [Palik 1985]. While certainly not perfect, the generally good agreement suggests DFT may be a viable option at least for small energy loss. We found a practical limit of up to 100 eV. We have also been warned that such DFT calculations stop being reliable closer to 40 eV.

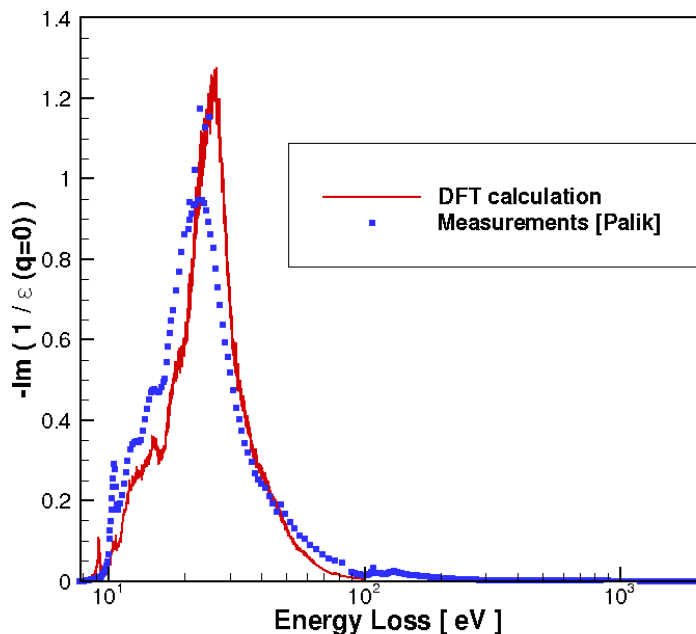


Figure 12. The energy loss function for SiO₂. The red curve is our DFT calculation while the blue dots are measurements from [Palik 1985].

We used FEFF9 to obtain electron energy loss spectra. To compare with the same data, we used a procedure [Ashley 1988, Ashley 1990, Dapor 2006] to convert the optical data into the energy loss spectra. The results are shown in Figure 13.

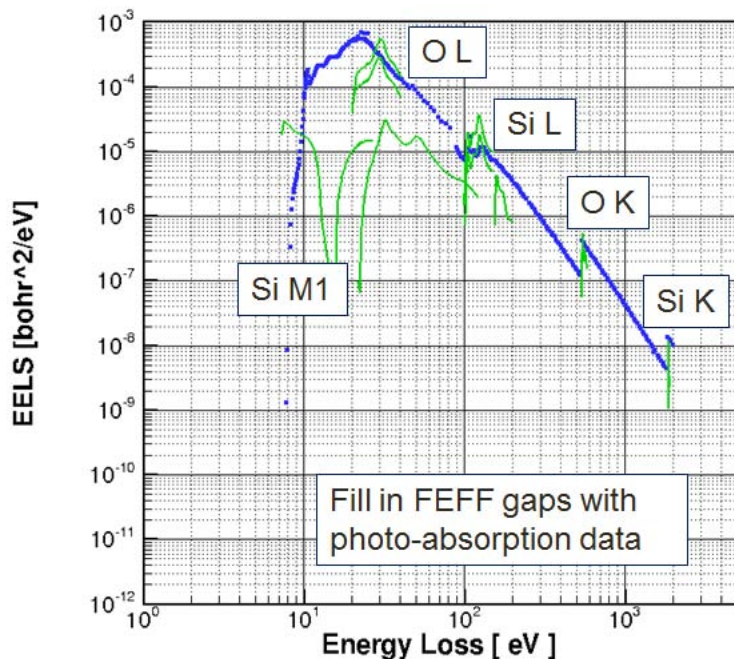


Figure 13. Energy loss spectrum for SiO₂. Green curves are our attempt to use FEFF9 for the various labeled transitions. Blue dots are adapted from [Palik 1985].

We acknowledge we have limited experience with FEFF9 and this should be kept in mind in the following discussion. Since we had difficulties in obtaining curves which span a large energy range, we broke this up into several calculations focusing near the edge transitions. The gaps in principle could be filled in with additional information, traditionally from data [Henke et al. 1993] though the EPDL [Cullen et al. 1997] should work as well. It should be pointed out that the imaginary part of the index of refraction is related to photoionization cross sections. Unfortunately, we ran out of time before we could perform this task. The normalization is spelled out in [Jin et al. 2010] where sum rules are used.

It should be pointed out more experienced FEFF users have been able to compute energy loss functions over even larger energy ranges [Sorini 2008]. Figure 14 shows in more detail the region near the Si L3 transition, True, FEFF9 is calculating the fine structure near the edge, but again the level of agreement seems disappointing. Again, our inexperience with FEFF9 may be playing a role here.

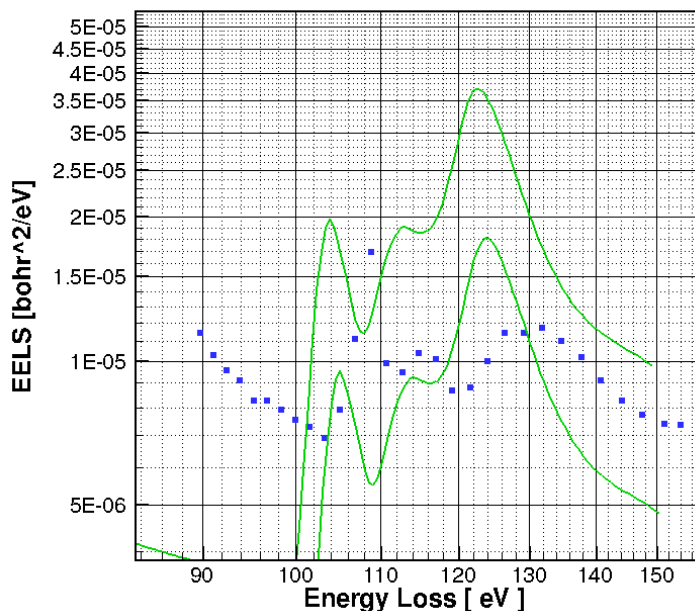


Figure 14. The electron energy loss spectra near the edge transition for Si L. The green curves are our calculations using FEFF9 for Si L3 (upper) and Si L2 (lower). The blue dots are adapted from measurements [Palik 1985] of the total transition.

Finally, in Figure 15, we show our DFT calculation, FEFF9 calculations, and the processed measurements. Perhaps we need more experience using FEFF9, or perhaps we can combine DFT results with information obtained for photoionization cross sections at higher energies to obtain essentially the electron energy loss function.

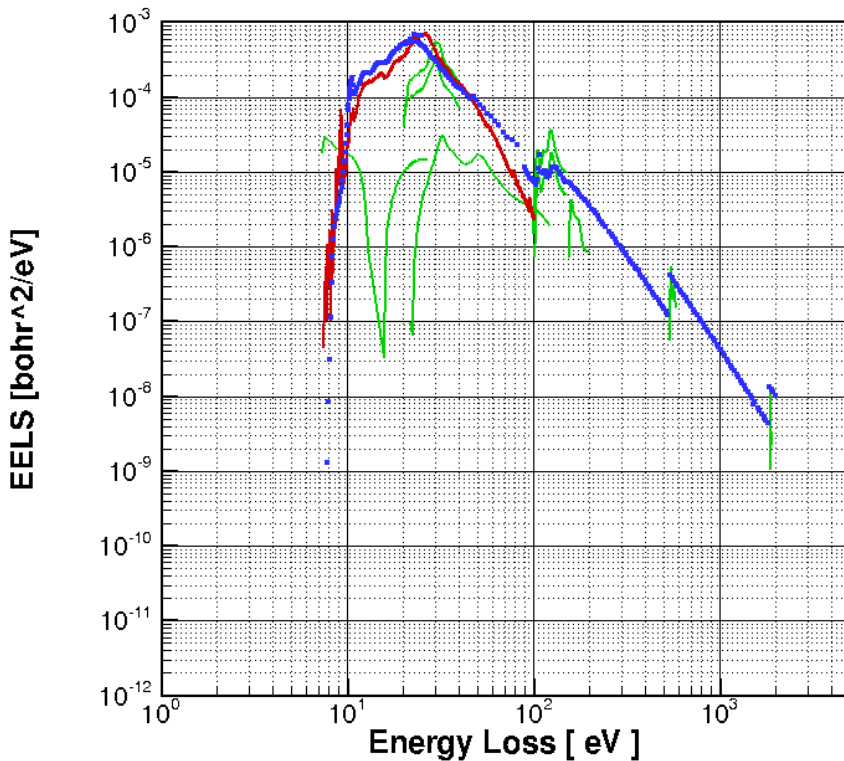


Figure 15. The electron energy loss spectra for SiO₂. Red curve is our DFT calculation. Green curves are our FEFF9 calculations for individual transitions. Blue dots are adapted from measurements [Palik 1985].

Even after this, we would then need to extrapolate into finite momentum transfer. While the sum rules (known values for certain integrals) do provide constraints, the assumed form of the extrapolation directly ties into the angular distribution of the scattering.

Identifying how much of the GOS surface involves plasmon creation is also important. Plasmons eventually decay into electron/hole pairs. This plays an important role when examining “secondary electron emission” (SEE) which is defined as those electrons emitted from a material with energies less than 50 eV. This provides a strong test for numerical techniques which must get the entire cascade right to simulate SEE. Several authors [Dapor 2012, Dapor 2011, Mao 2008, Walter 2008] are doing just that, with decidedly mixed results. While this may be in part due to the chosen extrapolation procedure, other reasons may be modeling other known low-energy physics such as phonon scattering (bulk and surface), polaron scattering (if this is real), surface barrier. There is still plenty to sort out.

It is also interesting to note band-structure calculations have a role to play at low energies [Schreiber and Fitting 2002].

7. CONCLUSIONS

In this project, we have attempted to improve low-energy electron/photon transport by incorporating atomic structure into the generation of cross sections. The greatest success was for photon coherent scattering resulting in noticeable diffraction modifications to the angular distributions. However, the impact should not be oversold as photon coherent scattering rarely dominates in most calculations. Also, the methods utilized here start from the assumption that an atomistic model of the material of interest can be generated. This may be no easy task for complicated structures. Also, we were unsuccessful in performing a DFT calculation with a repeat cell, performing the appropriate average over orientation, and comparing with our results. This should be better understood.

For electron elastic scattering, we demonstrated solid-state effects could be mimicked by treating a chunk of the material as essentially a large molecule. The attempt to modify the radial potential in a similar way was unsuccessful, and the root cause has not been identified. This should be pursued to at least identify if the idea was simply misguided or if some blunder has been overlooked. Things became murkier when we performed a straightforward application which was meant to demonstrate the possible importance of including molecular effects in nitrogen cross sections. The results seemed to indicate it was better not to use them. This suggests we need more experience investigating other molecular effects.

We did demonstrate DFT may play a role in calculating electron energy loss functions at least for rather low (up to 40 eV) energy losses. However, this is only one part of a complicated puzzle. Much work needs to be done to sort out which physics are important to model and how to do so in a reliable way.

We need more experience with the FEFF9 code. Given our level of agreement is quite poor compared with others' results, it is likely our inexperience is playing a role which makes proper assessment difficult.

We should better understand the role band-structure can play and what insights it might offer. Knowing when and how to transition between the various techniques would be desirable.

It should be pointed out time-dependent DFT may have much to offer in principle. As it stands, it is restricted to atomistic models of tens of atoms and to rather low energies, but something to keep an eye on.

8. PRESENTATIONS:

- International Conference on Transport Theory, Sept 17, 2013
“Low Energy Radiation Transport Applied to Secondary Electron Emission”,
H.P. Hjalmarson, R.P. Kensek, R.J. Magyar, R.J. Bondi

- APS March Meeting, 2012
“Secondary Electron Emission (SEE) Calculations”,
H.P. Hjalmarson, K.E.Kambour, R.P. Kensek

- Gordon Conference, 2011
“Exact Time-Dependent Kohn-Sham Potential for Interacting Few-Body Systems”
Rudolph J. Magyar

- APS March Meeting, 2011
“Exact Time-Dependent Kohn-Sham Potential for Interacting Few-Body Systems”
Rudolph J. Magyar

9. REFERENCES

- Ashley, J.C. (1988), "Interaction of low-energy electrons with condensed matter: stopping powers and inelastic mean free paths from optical data", *J. Electron Spectrosc. Relat. Phenom.* **46** pp 199-214.
- Ashley, J.C. (1990), "Energy loss rate and inelastic mean free path of low-energy electrons and positrons in condensed matter", *J. Electron Spectrosc. Relat. Phenom.* **50** pp 323-334.
- Bondi, R.J.; Lee, S. and Hwang, G.S. (2010), "First-principles study of the mechanical and optical properties of amorphous hydrogenated silicon and silicon-rich silicon oxide", *Phys. Rev. B* **81**, 195207.
- Brunger, W. and Menz, W. (1965), "Wirkungsquerschnitte für elastische und inelastische Elektronenstreuung an amorphen C- und Ge-Schichten", *Z. Phys.* **184**.
- Cullen, D.E.; Hubbell, J.H.; and Kissel, L. (1997) "EPDL97: the Evaluated Photon Data Library, '97 Version," Lawrence Livermore National Laboratory, UCRL-50400, Vol. **6**, Rev. 5.
- Dapor, M. (2012), "Monte Carlo simulation of secondary electron emission from dielectric targets", *J. Phys: Conference Series* **402** 012003.
- Dapor, M. (2011), "Secondary electron emission yield calculation performed using two difference Monte Carlo strategies", *Nucl. Instr. Meth. Phys. Res. B* **269** pp 1668-1671.
- Dapor, M. (2006), "A comparative study of electron and positron penetration in silicon dioxide", *J. Electron Spectrosc. Relat. Phenom.* **151** 182-192.
- Henke, B.L.; Gullikson, E.M. and Davis, J.C. (1993), "X-Ray Interactions: Photoabsorption, Scattering, Transmission, and Reflection at E=50-30000 eV, Z=1,92", *At. Data. Nucl. Data Tables* **54**, 181-342.
- Hirayama, H.; Namito, Y.; Bielajew, A.F.; Wilderman, S.J. and Nelson, W.R. (2005), *The EGS5 Code System*, SLAC-R-730 (2005) and KEK Report 2005-8 (2005).
- ICRU Report No. 77 (2007), "Elastic scattering of electrons and positrons", International Commission on Radiation Units and Measurements, Bethesda, MD.
- James, R.W. (1962), *The Optical Principles of the Diffraction of X-Rays*, (Ox Bow Press reprint)
- Jansen, R.H.J.; de Heer, F.J.; Luyken, H.J.; van Wingerden, B. and Blaauw, H.J. (1976), "Absolute differential cross sections for elastic scattering of electrons by helium, neon, argon and molecular nitrogen", *J. Phys B: Atom. Molec. Phys.* **9**(2), pp 185-211.

- Jenkins, T.M.; Nelson, W.R. and Rindi, A. [Editors] (1988), Monte Carlo Transport of Electrons and Photons, (Plenum Press).
- Jin, H.; Shinotsuka, H.; Yoshikawa, H.; Iwai, H.; Tanuma, S. and Tougaard, S. (2010), “Measurement of optical constants of Si and SiO₂ from reflection electron energy loss spectra using factor analysis method”, *J. Appl. Phys.* **107**, 083709.
- Jorissen, K.; Rehr, J.J. and Verbeeck, J. (2010), “Multiple scattering calculations of relativistic electron energy loss spectra”, *Phys. Rev.* **B 81**, 155108.
- King, B.W.; Landheer, K.A. and Johns, P.C. (2011), “X-ray coherent scattering form factors of tissues, water and plastics using energy dispersion,” *Phys. Med. Biol*, 56, pp. 4377-4397.
- Kissel, L.; Zhou, B.; Roy, S.C.; Sen Gupta, S.K. and Pratt, R.H. (1995), “The Validity of Form-Factor, Modified-Form-Factor and Anomalous-Scattering-Factor Approximations in Elastic Scattering Calculations,” *Acta Cryst.* **A51**, pp 271-288.
- Mao, S.F.; Li, Y.G.; Zeng, R.G. and Ding, Z.J. (2008), “Electron inelastic scattering and secondary electron emission calculated without the single pole approximation”, *J. Appl. Phys* **104**, 114907.
- Mattson, T.R.; Lane, M.D.; Cochrane, K.R.; Desjarlais, M.P.; Thompson, A.P.; Pierce, F. and Grest, G.S. (2010), “First-principles and classical molecular dynamics simulation of shocked polymers”, *Phys. Rev. B* **81**, 054103..
- Neuefeind, J. and Liss, K.-D. (1996), “Bond Angle Distribution in Amorphous Germania and Silica”, *Ber. Bunsenges. Phys. Chem.* **100**(8), pp. 1341-1349.
- Palik, E.D. (ed.) (1985), Handbook of Optical Constants of Solids, (Academic Press, Orlando).
- Peplow, D.E. and Verghese, K. (1998), “Measured molecular coherent scattering form factors of animal tissues, plastics and human breast tissue”, *Phys. Med. Biol.* **43**, pp 2431-2452.
- Perkins, S.T.; Cullen, D.E. and Seltzer, S.M. (1991), “Tables and Graphs of Electron-Interaction Cross Sections from 10 eV to 100 GeV Derived from the LLNL Evaluated Data Library (EEDL), Z=1,100”, Lawrence Livermore National Laboratory, UCRL-50400 Vol. 31.
- Plagemann, K.-U.; Sperling, P.; Thiele, R.; Desjarlais, M.P.; Fortmann, C.; Doppner, T.; Lee, H.J.; Glenzer, S.H. and Redmer, R. (2012), “Dynamic structure factor in warm dense beryllium”, *New J. Phys.* **14**, 055020.
- Poulsen, H.F.; Neuefeind, J.; Neumann, H.-B.; Schneider, J.R. and Zeider, M.D. (1995), “Amorphous silica studied by high energy X-ray diffraction,” *J. Non-Cryst. Solids* **188** pp 63-74.

- Rehr, J.J.; Kas, J.J.; Vila, F.D.; Prange, M.P. and Jorissen, K. (2010), "Parameter-free calculations of X-ray spectra with FEFF9", *Phys. Chem. Chem. Phys.* **12**(21) 5503-5513.
- Salvat, F.; Jablonski, A. and Powell, C.J. (2005), "ELSEPA – Dirac partial-wave calculation of elastic scattering of electrons and positrons by atoms, positive ions, and molecules", *Comp. Phys. Comm.* **165**, pp 157-190.
- Schreiber, E. and Fitting, H.-J. (2002) "Monte Carlo simulation of secondary electron emission from the insulator SiO₂", *J. Electron Spectrosc. Relat. Phenom.* **124** pp 25-37.
- Seltzer, S.M. (1991), "Electron-Photon Monte Carlo Calculations: The ETRAN Code", *Appl. Radiat. Isot.* **42** (10), pp 917-941.
- Sorini, A.P. (2008) "The Passage of Fast Electrons Through Matter", PhD thesis, U. Washington.
- Sorini, A.P.; Kas, J.J.; Rehr, J.J.; Prange, M.P. and Levine, Z.H. (2006) "Ab initio calculations of mean free paths and stopping powers", *Phys. Rev. B.* **74**, 165111.
- Spielman, R.B.; Deeney, C.; Chandler, G.A.; Douglas, M.R. and Fohl, D.L. (1998), "Tungsten wire-array Z-pinch experiments at 200 TW and 2 MJ", *Phys. Plasmas* **5** pp. 2105-2111.
- Tsige, M.; Curro, J.G. and Grest, G.S. (2003), "Molecular Dynamics Simulations and Integral Equation Theory of Alkane Chains: Comparison of Explicit and United Atom Models", *Macromolecules* **36**, pp 2158-2164.
- Walker, C.G.H.; El-Gomati, M.M.; Assa'D, A.M.D and Zadrazil, M. (2008), "The secondary electron emission yield for 24 solid elements excited by primary electrons in the range 250-5000 eV: A theory/experiment comparison", *Scanning* **30** pp 365-380.
- Warren, B.E. (1990), X-Ray Diffraction, (Dover) (reprint of 1969 edition).

DISTRIBUTION

Electronic copies only:

1	MS1159	Robert J. Bondi	01344
1	MS1179	Leonard J. Lorence	01341
1	MS1179	Martin J. Crawford	01341
1	MS1179	Brian C. Franke	01341
1	MS1179	Harold P. Hjalmarson	01341
1	MS1179	Ronald P. Kensek	01341
1	MS1179	Thomas W. Laub	01341
1	MS1322	Rudolph J. Magyar	01322
1	MS0899	Technical Library	9536 (electronic copy)
1	MS0359	D. Chavez, LDRD Office	1911

